JOURNAL OF THERMOPHYSICS AND HEAT TRANSFER
Vol. 10, No. 2, April–June 1996

Kinetics of Nitric Oxide Formation Behind Shock Waves

Charles E. Treanor*
Calspan—University at Buffalo Research Center, Buffalo, New York 14225
Igor V. Adamovich†
Ohio State University, Columbus, Ohio 43210
Marcia J. Williams‡
Calspan—University at Buffalo Research Center, Buffalo, New York 14225
and
J. William Rich§
Ohio State University, Columbus, Ohio 43210

The infrared radiation of nitric oxide (NO) behind a shock wave in O_2–N_2 mixtures has been calculated by two different techniques, and compared with recent shock-tube experiments. The first technique (model I) utilizes the Park model. This model incorporates the vibrational relaxation of O_2 and N_2 and assumes a Boltzmann distribution of vibrational energy during the relaxation process. Model II uses a master equation solution, employing recently published state-to-state vibration–translation and vibration–vibration transition probabilities. Vibration–chemistry coupling is provided through the Macheret–Fridman–Rich model (MFR). The calculations are compared with experimental results for shock waves in the range of 3–4 km/s. Results of the two model calculations are compared at speeds up to 9 km/s, for both normal shocks and bow shocks. The two models predict nearly the same NO production rates behind all of the normal shocks, and show the prominent effect of N_2 vibrational coupling in the reaction $N_2 + O \rightarrow NO + N$. For high-altitude bow shocks, where extreme vibrational nonequilibrium is present, there are large differences in the results calculated by the Park and MFR coupling techniques.

Nomenclature

AB(v)	=	molecule AB in vibrational level v
E_a	=	reaction activation energy, K
E_v	=	energy of the vth vibrational level, K
$F(E_v)$	=	threshold translational energy for dissociation from level v, K
k_i	=	chemical reaction rate for reaction i, cm^3/molecule s
L	=	optical path length, cm
n_{NO}	=	number density of NO molecules, cm^{-3}
S	=	observed in-band infrared radiation, W/cm^2 sr
s	=	parameter in Park model
T	=	translational temperature, K
W	=	energy parameter, Eq. (16), K
α	=	mass ratio factor
β	=	energy fraction that goes into vibration in reverse reaction
τ_{inc}(NO)	=	observed incubation time (laboratory time) for NO production, μs
τ_{VT}(NO)	=	vibrational relaxation time at observed conditions (laboratory time), μs

Subscripts

f	=	final
i	=	initial
st	=	stagnation point

Presented as Paper 95-2061 at the AIAA 29th Thermophysics Conference, San Diego, CA, June 19–22, 1995; received Aug. 2, 1995; revision received Dec. 6, 1995; accepted for publication Dec. 6, 1995.

*Executive Staff, P.O. Box 400. Fellow AIAA.
†Visiting Scholar, Department of Mechanical Engineering, 206 West 18th Avenue. Member AIAA.
‡Research Scientist, P.O. Box 400. Senior Member AIAA.
§Professor, Department of Mechanical Engineering, 206 West 18th Avenue. Associate Fellow AIAA.

I. Introduction

THE contribution of vibrational energy to the dissociation process in diatomic molecules is significant in many gas environments, such as high-enthalpy gasdynamic flows, molecular gas discharges, plasma chemical reactors, and upper-atmosphere chemistry. In shock-wave flows it has been the subject of many investigations, particularly under conditions of low density, where nonequilibrium conditions exist for an appreciable portion of the flow. It remains the goal of hypersonic flow simulation to develop programs that contain the proper physics of this interaction, while retaining tractable numerical complexities.

The most important approximation made in computing nonequilibrium flows[1] is the assumption that each degree of freedom of a molecule retains a Boltzmann-like distribution during chemical reaction processes. This assumption permits great simplifications in the formulation of the gasdynamic equations. For the translational and rotational degrees this assumption is valid over a wide range of flow conditions, since these degrees exchange energy readily in molecular collisions. However, for the vibrational degree, many collisions are required to transfer a single quantum of energy, and the vibrational distribution can easily become non-Boltzmann during relaxation processes.

The extent of this variation, and the effect it has on observed chemical reaction rates, depends on the values of the state-to-state vibrational transition probabilities. These rates have recently been calculated for nitrogen and oxygen.[2,3] They can be used in master equation shock-wave calculations, along with a rational vibration–chemistry coupling scheme,[4–6] to calculate vibrational energy distributions and chemical reaction rates behind shocks. It is the purpose of this article to present such calculations and compare them with experimental results and with calculations that assume a Boltzmann distribution. Section II contains a brief description of the experiment that was used for comparison. Section III describes the modeling that was employed, and Sec. IV presents the results of the calculations and comparisons. A Summary is provided in Sec. V.

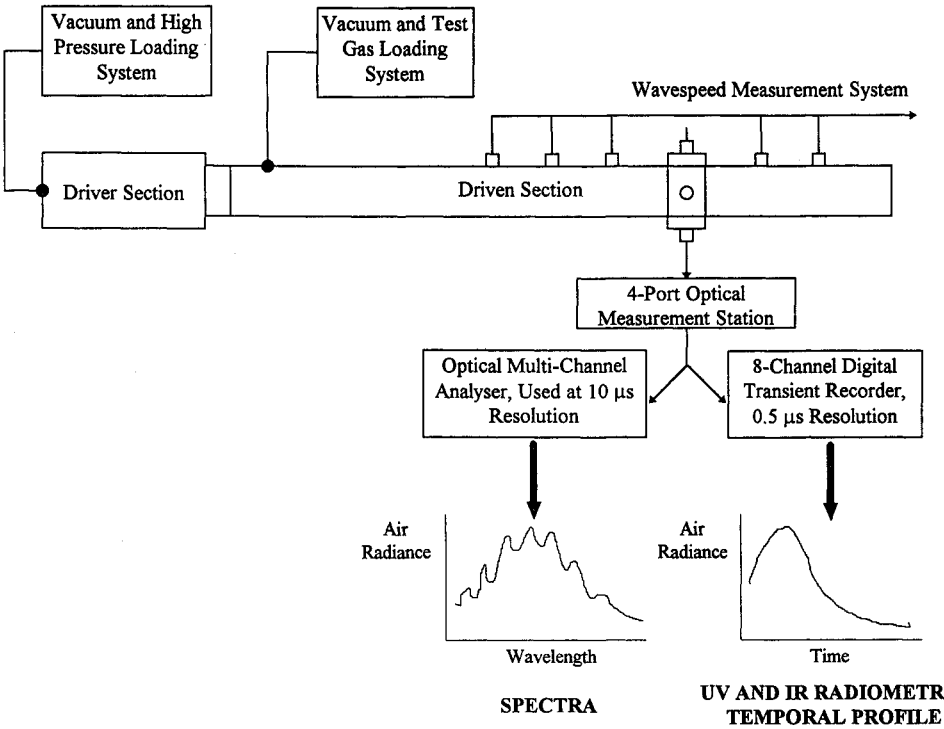

Fig. 1 Principal elements of the shock-tube radiation experiment.

II. Experimental

The experimental results that were used for comparison with the present calculations are described in detail in Refs. 7 and 8. For completeness, a brief summary of the experiment and previous analysis is presented here.

The time-history of infrared (IR) radiation behind a normal shock was measured using a pressure-driven shock tube with a 3-in. (7.62-cm) i.d. The driver section of the shock tube is 5 ft long, and was operated at pressures of up to 4000 psi (260 atm) of hydrogen. The routine double-diaphragm technique provided excellent run-to-run reproducibility in wave speed (~1%) and radiation records. Initial test gas pressures were measured to better than 1% with a MKS Baratron unit. Scientific grade (99.999%) O_2 and N_2 were used throughout, and were premixed in three different proportions for the experiments. Ultraviolet radiation measurements were also taken during the experiments. The principal elements of the shock-tube experiment are shown in Fig. 1 (taken from Ref. 7).

An indium antimonide (InSb) detector was used in the radiometer to measure the NO IR radiation behind the shock wave. It was found that even though the long-wave rolloff of the detector response clips one wing of the NO band, the high detectivity resulted in an excellent signal-to-noise ratio,[8] better than that obtained in earlier experiments with HgCdTe.[7] The combined filter–detector bandpass function, between 5–5.5 μm, was determined by separate bench experiments. A standard blackbody source through a scanning monochromator was calibrated and then used to establish the wavelength dependence of the radiometer. System calibration was achieved by means of a chopped, standard blackbody, which completely filled the field of view and whose intensity spanned the range of those for the test gases. The system was linear over this range.

As described in Ref. 8, Appendix D, the observed in-band IR radiation is related to the NO concentration and the gas translational temperature through the relation

$$S = 1.29 \times 10^{-20} \cdot L \cdot n_{NO}[1 - 3.21 \times 10^{-4}(T - 3000)] \text{ W/cm}^2 \cdot \text{sr} \quad (1)$$

For these experiments the optical path length, L, the shock-tube diameter, had the value of 7.62 cm. This equation is consistent with the equilibrium values of NO radiation measured in the shock tube and with the known band strength of the molecule. It was used to relate the measurements of nonequilibrium radiation to the nonequilibrium NO molecular density.

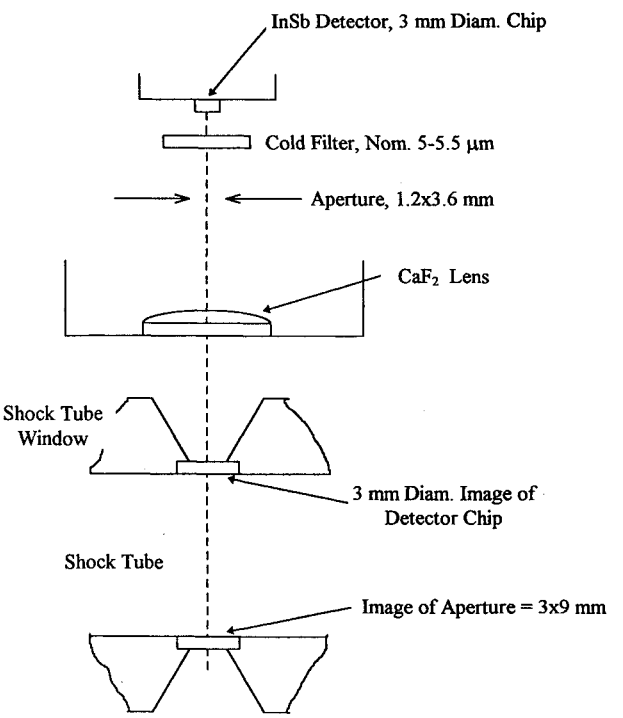

Fig. 2 Major elements of the IR radiometer—shock-tube system. The beam in the shock tube is wedge shaped, optimized for axial resolution at 3 mm, and for throughput by a 9 mm width across the tube at the lower window.

The optical system used in the experiment was designed to produce a sharp definition of the region behind the shock wave contributing to the radiation received by the detector at any given time, and to avoid reflections that would provide spu-

rious signals. As illustrated in Fig. 2, taken from Ref. 8, the physical apertures (the InSb detector and a razor-blade slit) are both external to the shock tube, and each provides a 3-mm image on a shock-tube window. The external placement precludes any reflections from the apertures. With shock speeds of 3–4 mm/μs, this results in a temporal resolution of 1 μs in the data.

Analysis of the data[9] determined an optimum set of rate coefficients chosen from available measured values. These rates are also used in this article.

III. Kinetic Modeling

To simulate the kinetics of NO formation behind normal shock waves, we have used nonequilibrium-flow, master-equation modeling, herein called model II. The kinetic model incorporates 1) the equations of one-dimensional gasdynamics for nonequilibrium reacting real gases[10]; 2) chemical kinetics equations for reacting species N, N_2, O, O_2, and NO; and 3) master equations for populations of vibrational levels of each diatomic species. The chemistry–vibration coupling terms are incorporated into both the chemical kinetics equations and the master equation, while the effects of relaxation and chemical reactions are taken into account in the energy and motion equations. Thus, the system of equations used is completely self-consistent. The explicit form of the equations in items 2 and 3 can be found in an earlier publication.[11]

It is assumed that the gas mixture components participate in the following dissociation reactions:

$$N_2(v) + M \leftrightarrows N + N + M \tag{2}$$

$$O_2(v) + M \leftrightarrows O + O + M \tag{3}$$

$$NO(v) + M \leftrightarrows N + O + M \tag{4}$$

and in Zel'dovich mechanism reactions

$$N_2(v) + O \leftrightarrows NO + N \tag{5}$$

$$O_2 + N \leftrightarrows NO(v) + O \tag{6}$$

In Eqs. (2–4), M stands for a collision partner, and v is the vibrational quantum number. The notation AB(v) in a reaction equation shows that the effect of vibrational excitation of molecule AB on the rate of an endoergic reaction is taken into account. The rates of reactions (2–6) in thermal equilibrium are taken the same as in Ref. 11, where they were incorporated from Refs. 12 and 13:

$$k_1 = 8.0 \times 10^{-7} \cdot T^{-0.5} \cdot \exp(-113{,}200/T), \quad M = N_2 \tag{7}$$

$$k_2 = 5.4 \times 10^{-5} \cdot T^{-1.0} \cdot \exp(-59{,}380/T), \quad M = O_2 \tag{8}$$

$$k_3 = 6.6 \times 10^{-4} \cdot T^{-1.5} \cdot \exp(-75{,}490/T), \quad \text{for any } M \tag{9}$$

$$k_4 = 3.0 \times 10^{-10} \cdot \exp(-38{,}016/T) \tag{10}$$

$$k_5 = 2.2 \times 10^{-14} \cdot T \cdot \exp(-3565/T) \tag{11}$$

The rates of N_2 dissociation on other collision partners are $15 \cdot k_1$ for M = N, and $0.4 \cdot k_1$ for M = O, O_2, and NO; the rates of O_2 dissociation are $2.8 \cdot k_2$ for M = O, and $0.22 \cdot k_2$ for M = N, N_2, and NO (see Ref. 9). All the rates of Eqs. (7–11) are given in cm^3/mol·s.

The rates of nonequilibrium dissociation and bimolecular reactions (2–6) are evaluated according to the classical impulsive model by MFR (Refs. 4–6). According to this model, the state-specific rate is given by the equation

$$k(v, T) = A(T) \cdot \exp[-F(E_v)/T] \tag{12}$$

where $A(T)$ is a factor obtained from normalization on the thermal reaction rate. The threshold energy (or threshold curve), determined for reactions of dissociation[5] and for bimolecular reactions,[4] is also a function of the reaction activation energy and masses of collision partners. For example, for the endoergic exchange reaction

$$AB(v) + C \rightarrow A + BC \tag{13}$$

one has[4]

$$F(E_v) = \begin{cases} W + \dfrac{1}{1-\alpha}[(E_a - W)^{1/2} - (\alpha E_v)^{1/2}]^2, & \text{if } E_v \le \dfrac{E_a - W}{\alpha} \\ W, & \text{if } E_v > \dfrac{E_a - W}{\alpha} \end{cases} \tag{14}$$

In Eq. (14), E_a is the reaction activation energy,

$$\alpha = \frac{m_B(m_A + m_B + m_C)}{(m_A + m_B)(m_B + m_C)} \tag{15}$$

and W can be found from the relation

$$\beta = \alpha \cdot (1 - W/E_a) \tag{16}$$

where β is the energy fraction that goes into vibrations in the reverse exoergic reaction; for reaction (5), this parameter is measured to be $\beta = 0.25$ (Ref. 14). One can see from Eq. (14) that $F(E_v) \ge E_a - E_v$, which is also true for dissociation.[5]

The rates for vibration–translation (V–T)

$$AB(i) + M \leftrightarrows AB(f) + M \tag{17}$$

and vibration–vibration (V–V)

$$AB(i_1) + CD(i_2) \leftrightarrows AB(f_1) + CD(f_2) \tag{18}$$

processes, used in the master equation, are evaluated according to the nonperturbative semiclassical analytic model of the forced harmonic oscillator (FHO).[2,3] The FHO model rates were shown to agree very well with the results of the state-of-the-art close-coupled calculations[15–17] and recent experiments.[18–20] The model is applicable up to very high temperatures, high vibrational quantum numbers, and also for multiquantum transitions. Separate cross sections for vibrational energy transfer from oxygen and nitrogen atom collisions have not been taken into account. Under conditions of appreciable dissociation, these reactions have been shown[21] to have an effect on the vibrational distribution of N_2.

To compare the present master equation model with kinetic models commonly used in nonequilibrium hypersonic aerodynamics calculations, we also ran a code based on simplified vibrational and chemical kinetics.[9] It incorporates one equation for the vibrational energy of each diatomic species [the vibrational energy distribution function (VDF) is therefore assumed to be Boltzmann with vibrational temperature T_v]. The rates of nonequilibrium chemical reactions [forward reactions (2–5)] are calculated according to the Park model,[1]

$$k(T, T_v) = k_{eq}(T^s \cdot T_v^{1-s}), \qquad s = 0.7 \tag{19}$$

where k_{eq} is the equilibrium rate constant at $T = T_v$, given by Eqs. (7–11). This model will be called model I throughout the remainder of this article, whereas the master equation model will be referred to as model II.

Model I has been previously validated by comparing the predicted and the experimental[8] NO radiation profiles behind

the shock for shock velocities u_s = 3–4 km/s, showing good overall agreement.[9] However, model I is based on experimental relaxation data, available only for not too high temperatures, and on the empirical nonequilibrium reaction rate model of Eq. (19). Therefore, it has no predictive capability for the modeling of gas flows behind strong shocks at $u_s > 4$ km/s. On the other hand, model II, which incorporates validated nonperturbative relaxation rate models and nonempirical impulsive rate models of nonequilibrium chemical reactions, can be used up to high temperatures. Note, however, that the use of parameter $\beta = 0.25$, measured at T ~ 300 K (Ref. 14), at high temperatures needs to be validated by comparing the rate of Eqs. (12) and (14) and the results of trajectory calculations, where available.

In the normal shock calculations, the initial conditions for the translational temperature, pressure, density, and gas velocity immediately behind the shock are given by the Rankine–Hugoniot normal shock relations. The initial VDF for each of the diatomic species is a Boltzmann distribution with the vibrational temperature assumed to be equal to the gas temperature before the shock. The initial concentrations of N, O, and NO are taken to be negligibly small, except for the bow-shock calculation at a 100 km altitude, where oxygen in the incoming flow was assumed to be partially photodissociated.

The systems of equations are solved using the standard routine LSODE, the efficient integrator of stiff ordinary differential equations.[22]

IV. Results and Discussion

To validate the use of model II with kinetic rates described in the previous section for very strong shocks (u_s = 7–9 km/s), we first compared its predictions with experiments at lower shock velocities, u_s = 3–4 km/s (Ref. 8). To obtain the NO IR signal intensity from the calculated concentration of nitric oxide, we used the results of IR spectral analysis, calibrated on the equilibrium NO radiation, measured in the experiment (see Ref. 9 for details). The absolute intensity of the IR signal S/L in W/cm^3 · sr is calculated from Eq. (1).

Figures 3 and 4 show typical experimental time-dependent IR signals behind the shock, for the low (u_s = 3.06 km/s) and the high (u_s = 3.85 km/s) shock velocities, respectively. In both cases the conditions before the shock are T_0 = 300 K, P_0 = 2.25 torr (which corresponds to a 40 km altitude), giving the conditions behind the shock T_1 = 4900 K, P_1 = 210 torr, and T_1 = 7400 K, P_1 = 320 torr, respectively. Also shown in Figs. 3 and 4 are results of calculations by models I and II. One can see that in both cases the predictions of the two models agree well with the experiment.

At the low shock velocity u_s ~ 3 km/s, one can clearly see that NO radiation is delayed by τ_{inc}(NO) (see Fig. 3). The incubation time, plotted in Fig. 5 against the nitrogen fraction in the mixture, reaches τ_{inc}(NO) ~ 20 μs at u_s = 2.97 km/s in an N_2–O_2 = 95%/5% mixture. At these temperatures (T = 4000–5000 K for u_s ~ 3 km/s), the nitrogen vibrational relaxation time $\tau_{VT}(N_2)$ ~ 30 μs is much longer than both the vibrational relaxation time of O_2, $\tau_{VT}(O_2)$ ~ 1 μs and the O_2 dissociation incubation time, $\tau_{inc}(O_2)$ ~ 1 μs. This proves that the bottleneck for the NO production at a shock velocity of u_s ~ 3 km/s is reaction (5), because of vibration–chemistry coupling, rather than because of oxygen dissociation. The same effect, although not seen in the experiments at higher shock velocities because of the limited time resolution of about 1 μs, has been observed in all normal shock calculations for u_s = 3–4 km/s. At the high shock velocities, u_s ~ 4 km/s, there exists the well-known overshoot in radiation intensity before the reverse reactions (5 and 6) take over and the NO concentration reaches equilibrium (see Fig. 4).

Calculations made for 16 experimental conditions (u_s = 3–4 km/s) in three N_2–O_2 mixtures (95/5%, 78/22%, and 60/40%) all show good agreement between experimental and calculated radiation signals. For example, Figs. 6 and 7 show the

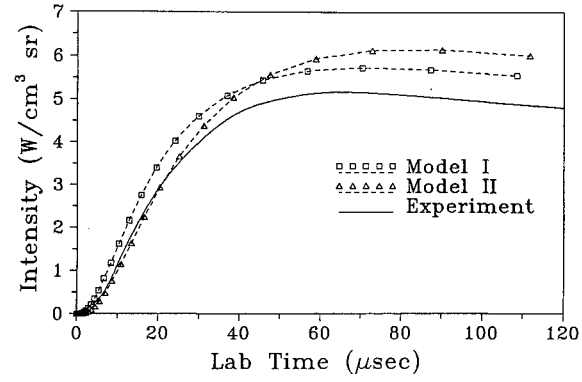

Fig. 3 Experimental and calculated NO IR radiation profiles behind the normal shock. N_2:O_2 = 60:40, u_s = 3.06 km/s, P_0 = 2.25 torr.

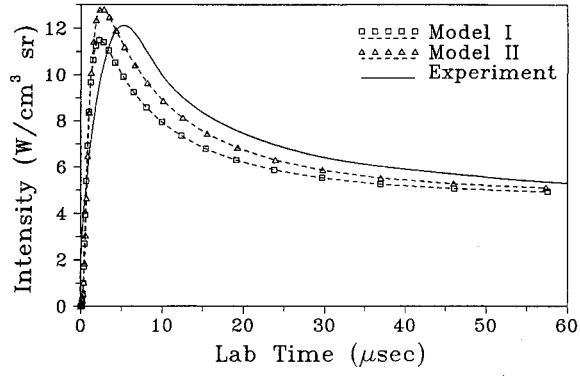

Fig. 4 Experimental and calculated NO IR radiation profiles behind the normal shock. N_2:O_2 = 77.7:22.3, u_s = 3.85 km/s, P_0 = 2.25 torr.

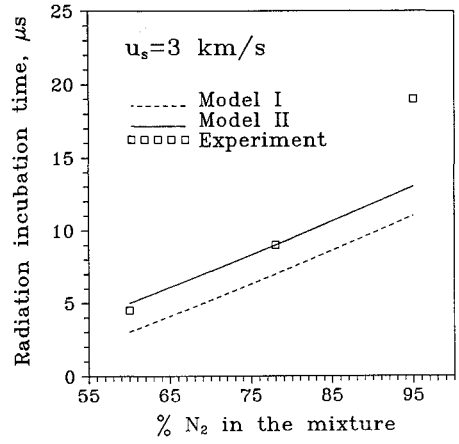

Fig. 5 Experimental and calculated NO IR radiation incubation time at u_s = 3 km/s as a function of the nitrogen mole fraction in the mixture.

experimental and calculated radiation rise time (time to signal half-maximum), as functions of shock velocity, for two different N_2–O_2 mixtures. Also, the results of calculations did not reveal any substantial differences between the predictions of models I and II, which were quite close for all considered experimental conditions. This is expected for two reasons.

1) Nonequilibrium rates of dissociation and of bimolecular reactions (2–6) by the MFR model can be approximated fairly well by the Park formula [Eq. (19)], except for the case of extreme disequilibrium $T_v/T < 0.1$ [see Ref. 23 for dissociation reactions (2) and (3) and Fig. 8 for reaction (5)].

2) For the temperatures $T < 8000$ K, the effect of multiquantum relaxation on the VDF of N_2 and O_2 is not very dra-

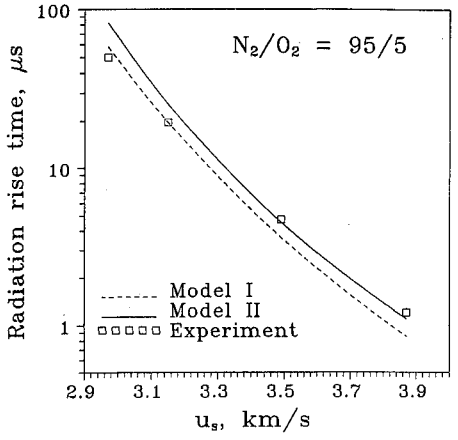

Fig. 6 NO IR radiation rise time (time to the half-maximum) as a function of the shock velocity. N_2:O_2 = 95:5.

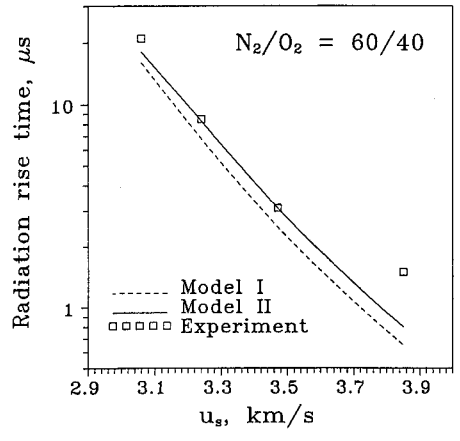

Fig. 7 NO IR radiation rise time (time to the half-maximum) as a function of the shock velocity. N_2:O_2 = 60:40.

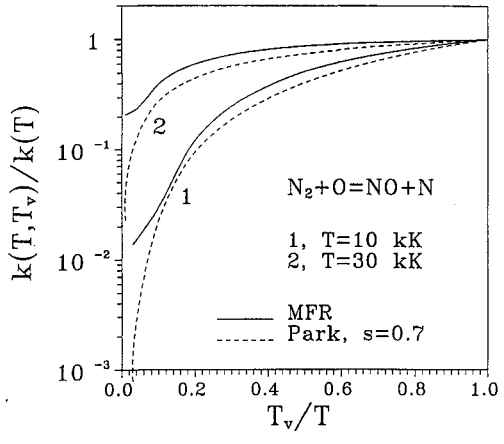

Fig. 8 Nonequilibrium rate of reaction (5) according to the MFR and the Park models.

matic, so that the VDF, calculated by the state-to-state kinetic model (model II), is Boltzmann-like. A considerable deviation from a Boltzmann distribution occurs only at $T_v/T \ll 1$ for the high vibrational levels, when their populations are very low. Finally, since at these temperatures most of the NO behind the normal shock is produced at $T_v(O_2)/T > T_v(N_2)/T > 0.4$, both models should give close results, as they actually do.

To compare the predictions of Models I and II at very high shock velocities, we ran the normal shock code for air at u_s = 9 km/s, T_0 = 220 K, and P_0 = 40 mtorr (these conditions correspond to a 70 km altitude). Note that in this case the first-

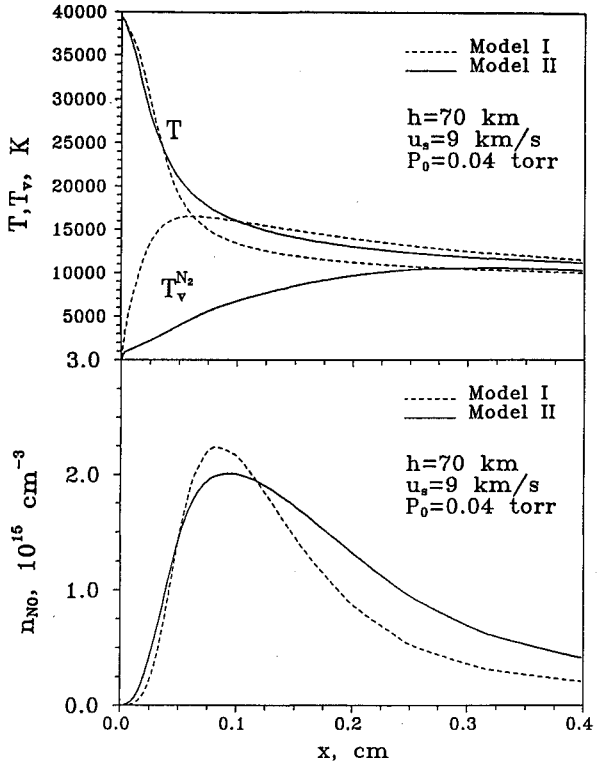

Fig. 9 Vibrational relaxation and NO production behind a strong normal shock. h = 70 km, u_s = 9 km/s, and P_0 = 40 mtorr.

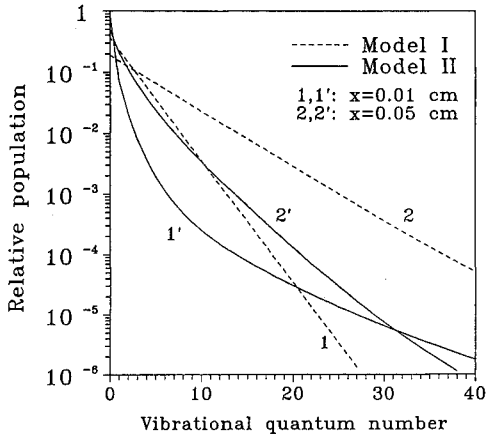

Fig. 10 Vibrational distribution function of N_2, calculated by models I and II for the conditions of Fig. 9.

order vibrational relaxation model used in model I, and based on the low-temperature experimental data, has no predictive capability and may be not applicable at all. Indeed, Fig. 9 shows that the vibrational temperature of nitrogen, predicted by model I, is several times higher than the temperature of the first vibrational level,

$$T_v^{N_2} = \frac{\omega_e(1 - 2x_e)}{\ell n(f_0/f_1)} \tag{20}$$

as given by model II. In Eq. (20), f_0 and f_1 are relative populations of vibrational levels v = 0 and v = 1, respectively. Figure 10 compares the VDFs calculated by the two models, showing that the Model II VDF is strongly non-Boltzmann and that the relative populations of high vibrational levels, predicted by model II, are generally lower. One might expect the NO production rate given by model II to be also lower than given by model I. However, one can see from Fig. 9 that the

predictions of NO production by the two models are again very close.

The reasons for this behavior are as follows. First, molecular dissociation at these high temperatures ($T > 20{,}000$ K in the region of the most intensive NO production $x < 0.05$ cm) is very rapid. The dissociation rates in this region only weakly depend on the vibrational temperature, while the rates for N_2 and O_2 dissociation become comparable (see Ref. 23). Dissociation therefore becomes the major source of both N and O atoms, so that the Zel'dovich mechanism reactions (5) and (6) are no longer coupled in a chain. Under these conditions, NO is produced mainly in the second Zel'dovich reaction (6), which has very low activation energy, and therefore, is not vibrationally stimulated. Second, at these high temperatures the rate of another NO-producing reaction, the vibrationally induced reaction (5), also weakly depends on the vibrational temperature or on the VDF (see Fig. 8). Obviously, when the gas temperature is comparable to the reaction activation energy [$E_a \approx 38{,}000$ K for reaction (5)], a considerable part of all N_2 molecules can react with O atoms, regardless of how much vibrational energy they have. Thus, NO production behind strong shocks is very weakly coupled to the vibrational energy of the gas.

A considerable difference between the two model predictions does occur in the first stage of relaxation when $T_v/T \ll 1$. The model II NO production rate in this region exceeds the prediction of model I by as much as an order of magnitude (not seen in Fig. 9 because the rates are small). This effect is because of the unphysical behavior of the Park model chemical reaction rates (19), incorporated in model I, at $T_v/T \to 0$, when they tend to zero (see Ref. 23 and Fig. 8). However, this effect is strongly overshadowed by the much greater amount of NO produced in the less nonequilibrium stage (at higher T_v/T ratio), where the prediction of both models are getting much closer.

The effect of the reaction rate behavior at extreme vibrational disequilibrium (when $T_v/T \ll 1$), first studied by Boyd et al.,[23] may be very dramatic for low-density bow shocks, where there is no clearly defined shock wave. To separately estimate the sensitivity of the NO production rate to the chemical reaction and vibrational relaxation rate models, we used the results of the direct simulation Monte Carlo (DSMC) bow shock flowfield calculations.[23] In the following calculations, the gas velocity, temperature, and pressure along the stagnation streamline (see Figs. 11 and 12) were used as input data for the overlay modeling of vibrational relaxation and chemical reactions in the gas flow on this streamline. This uncoupled approach assumes that the resulting variations in N, O, and NO mole fractions are quite small and do not substantially perturb the flowfield. It is also assumed that the use of the forced harmonic oscillator (FHO) model, rather than the more simplified vibrational–relaxation model incorporated in the DSMC calculations,[23] would not change the flowfield since both models predict very close vibrational relaxation times τ_{VT} (Ref. 11).

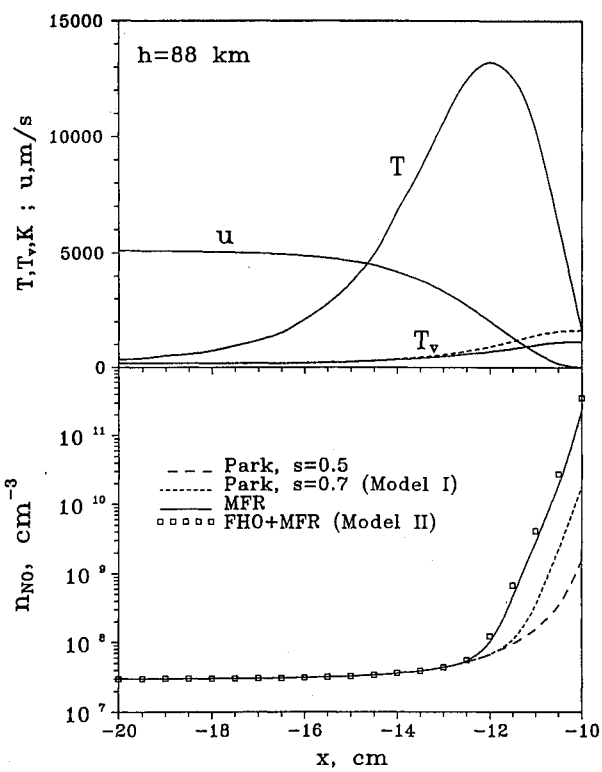

Fig. 11 DSMC flowfield data (upper part), and the NO concentration (lower part) on the stagnation streamline. h = 88 km, u_s = 5 km/s, and P_0 = 1.9 mtorr. The two curves for $T_v^{N_2}$ in the upper part are predicted by model I (dashed curve) and model II (solid curve).

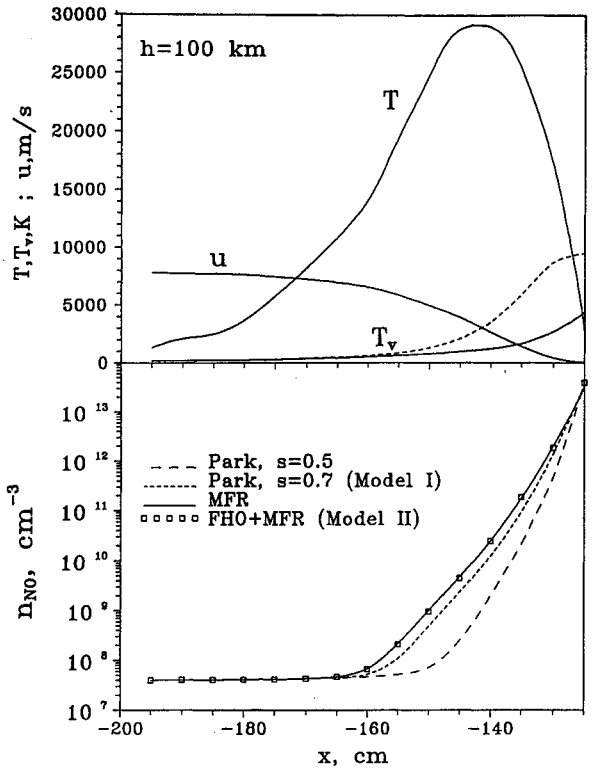

Fig. 12 DSMC flowfield data (upper part), and the NO concentration (lower part) on the stagnation streamline. h = 100 km, u_s = 8 km/s, and P_0 = 1.6 mtorr. The two curves for $T_v^{N_2}$ in the upper part are predicted by model I (dashed curve) and model II (solid curve).

The input flowfield data and the results of the calculations for air at the two altitudes of 88 and 100 km are shown in Figs. 11 and 12, respectively. One can see that in both cases there exists a region of extreme vibrational disequilibrium, $T_v/T < 0.1$, while the stagnation point temperature is much less than the maximum gas temperature behind the shock, $T_{st}/T_{max} \sim 0.1$. In these calculations, we used four different kinetic models: 1) model II, 2) model I (both described in Sec. III), 3) model I with $s = 0.5$ instead of $s = 0.7$ in Eq. (19), and 4) model I with the MFR reaction rates instead of the Park rates of Eq. (19).

At an 88 km altitude (u_s = 5 km/s, see Fig. 11), the use of the MFR reaction rate model leads to a one and a two orders of magnitude increase in NO concentration, compared to the Park model (19) with $s = 0.7$ and $s = 0.5$, respectively. This result is in qualitative agreement with the three-dimensional DSMC calculations of Boyd et al.,[23] who use the MFR model for dissociation reactions only, and predict an order of mag-

nitude increase compared to the Park model with $s = 0.5$. The much faster NO production, predicted by the MFR model, compared to the Park model, occurs because of two equally important factors. First is the greater rate of oxygen dissociation at $T_v/T \to 0$, discussed in Ref. 23 and resulting in the earlier triggering of the Zel'dovich mechanism chain reactions (5) and (6), so that they occur at a higher translational temperature. Second is the higher rate of the key NO production reaction (5) in the region of extreme disequilibrium (see Fig. 8). One can also see that the NO production rate is only weakly sensitive (within a factor of 2) to the vibrational relaxation model (curves MFR and FHO + MFR in Fig. 11). This happens because the calculated vibrational temperature is so low that chemical reactions (2–6) proceed mainly from the ground vibrational level.

The main difference of NO production kinetics at a 100 km altitude ($u_s = 8$ km/s) is that there is already enough photodissociated oxygen in the incoming flow (~4% of the mixture).[23] Thus, delayed oxygen dissociation is no longer a trigger for the Zel'dovich mechanism reactions. Calculations at this altitude, shown in Fig. 12, therefore demonstrate only the effect of the variation of the reaction (5) nonequilibrium rate. One can see that the predictions of all the models are closer than at an 88 km altitude, giving about an order of magnitude difference between the Park $s = 0.5$ model and the MFR model. The predicted NO concentrations in the vicinity of the stagnation point are very close for all models. NO production here is compensated by its decomposition in the reverse reactions (5) and (6), so that NO mole fraction reaches a quasiequilibrium value and is not rate sensitive. Note that the overlay approximation in the stagnation point region is no longer valid, since NO model fraction here reaches several percent. Finally, the effect of the vibrational kinetics rate model on NO concentration is again negligibly small, because of the very low vibrational temperature in the region of the most intensive NO production.

V. Summary

In this article, we have analyzed nitric oxide production kinetics behind strong normal and bow shocks. The nonempirical self-consistent state-to-state kinetic model, described here (model II), was validated by comparison with shock-tube experiments, for the shock velocities $u_s = 3–4$ km/s. The results of the calculations illustrate, however, that a simplified kinetic model (model I) and the model II predict very close NO production rates behind normal shocks up to very high-shock velocities $u_s = 9$ km/s. This justifies the use of model I in normal shock calculations.

NO production kinetics behind bow shocks are simulated by an overlay modeling of the gas flow along the stagnation streamline, with the results of the DSMC flowfield calculations[23] used as inputs. The results of the overlay calculations support the idea of Boyd et al.[23] that correct modeling of vibration–dissociation coupling in extreme vibrational disequilibrium is one of the most crucial points in prediction of NO radiation behind the low-density bow shocks. Our data also show that taking into account the vibrational coupling in bimolecular reactions (5) and (6) is equally important. Satisfactory agreement obtained in Ref. 23 between the DSMC calculations and the flight data suggest the MFR dissociation and bimolecular reaction rate model for use in hypersonic aerodynamic calculations. On the other hand, these results demonstrate that the NO production rate is only weakly affected by the vibrational relaxation rate model. Also note that a reliable prediction of the NO ultraviolet radiation behind shocks requires additional studies of mechanisms of electronically excited NO formation, which are far from being understood at this time.

Acknowledgment

We express our sincere gratitude to Iain Boyd, who promptly made available to us the results of the DSMC bow-shock calculations.[23]

References

[1]Park, C., *Nonequilibrium Hypersonic Aerodynamics*, Wiley, New York, 1990, Chap. 3.

[2]Adamovich, I. V., Macheret, S. O., Rich, J. W., and Treanor, C. E., "Vibrational Relaxation and Dissociation Behind Shock Waves. Part 1: Kinetic Rate Models," *AIAA Journal*, Vol. 33, No. 6, 1995, pp. 1064–1069.

[3]Adamovich, I. V., Macheret, S. O., Rich, J. W., and Treanor, C. E., "Nonperturbative Analytic Theory of V-T and V-V Rates in Diatomic Gases, Including Multi-Quantum Transitions," AIAA Paper 95-2060, June 1995.

[4]Macheret, S. O., Fridman, A. A., and El'kin, A. A., "Rates Constants of Exchange Reactions in Nonequilibrium Conditions: Classical Model," *Khimicheskaya Fizika (Soviet Chemical Physics)*, Vol. 9, No. 2, 1990, pp. 174–179.

[5]Macheret, S. O., and Rich, J. W., "Nonequilibrium Dissociation Rates Behind Strong Shock Waves," *Chemical Physics*, Vol. 174, No. 1, 1993, pp. 25–43.

[6]Macheret, S. O., Fridman, A. A., Adamovich, I. V., Rich, J. W., and Treanor, C. E., "Mechanisms of Nonequilibrium Dissociation of Diatomic Molecules," AIAA Paper 94-1984, June 1994.

[7]Wurster, W. H., Treanor, C. E., and Williams, M. J., "Kinetics of UV Production Behind Shock Waves in Air," AIAA Paper 90-1666, June 1990.

[8]Wurster, W. H., Treanor, C. E., and Williams, M. J., "Non-Equilibrium Radiation from Shock-Heated Air," U.S. Army Research Office, Final Rept., Contract DAAL03-88K-0174, Calspan—Univ. of Buffalo Research Center, Buffalo, NY, July 1991.

[9]Treanor, C. E., and Williams, M. J., "Kinetics of Nitric Oxide Formation Behind 3 to 4 km/s Shock Waves," U.S. Army Research Office, Final Rept., Contract DAAL03-92K-0003, Calspan—Univ. of Buffalo Research Center, Buffalo, NY, Feb. 1993.

[10]Clark, J. F., and McChesney, M., *Dynamics of Real Gases*, Butterworths, London, 1976, Chap. 2.

[11]Adamovich, I. V., Macheret, S. O., Rich, J. W., and Treanor, C. E., "Vibrational Relaxation and Dissociation Behind Shock Waves. Part 2: Master Equation Modeling," *AIAA Journal*, Vol. 33, No. 6, 1995, pp. 1070–1075.

[12]Camac, M., Feinberg, R., and Teare, J. D., "The Production of Nitric Oxide in Shock-Heated Air," Avco Research Lab. Rept. 245, Everett, MA, Dec. 1966.

[13]Monat, J. P., Hanson, R. K., and Kruger, C. H., "Shock Tube Determination of the Rate Coefficients for the Reaction $N_2 + O \to NO + N$," *Proceedings of the 17th International Symposium on Combustion*, The Combustion Inst., Pittsburgh, PA, 1978, pp. 543–548.

[14]Black, G., Sharpless, R. L., and Slanger, T. G., "Measurements of Vibrationally Excited Molecules by Raman Scattering. I. The Yield of Vibrationally Excited Nitrogen in the Reaction $N + NO \to N_2 + O$," *Journal of Chemical Physics*, Vol. 58, No. 11, 1973, pp. 4792–4797.

[15]Billing, G. D., and Fisher, E. R., "VV and VT Rate Coefficients in N_2 by a Quantum-Classical Model," *Chemical Physics*, Vol. 43, No. 3, 1979, pp. 395–401.

[16]Billing, G. D., and Kolesnick, E. R., "Vibrational Relaxation of Oxygen. State to State Rate Constants," *Chemical Physics Letters*, Vol. 200, No. 4, 1992, pp. 382–386.

[17]Billing, G. D., "VV and VT Rates in N_2-O_2 Collisions," *Chemical Physics*, Vol. 179, No. 3, 1994, pp. 463–467.

[18]Price, J. M., Mack, J. A., Rogaski, C. A., and Wodtke, A. M., "Vibrational-State-Specific Self-Relaxation Rate Constant. Measurements of Highly Vibrationally Excited O_2 ($v = 19–28$)," *Chemical Physics*, Vol. 175, No. 1, 1993, pp. 83–98.

[19]Park, H., and Slanger, T. G., "O_2(X, $v = 8–22$) 300 K Quenching Rate Coefficients for O_2 and N_2, and O_2(X) Vibrational Distribution from 248 nm O_3 Photodissociation," *Journal of Chemical Physics*, Vol. 100, No. 1, 1994, pp. 287–300.

[20]Klatt, M., Smith, I. W. M., Tuckett, R. P., and Ward, G. N., "State-Specific Rate Constants for the Relaxation of $O_2(X^3\Sigma_g^-)$ from Vibrational Levels $v = 8$ to 11 by collisions with NO_2 and O_2," *Chemical Physics Letters*, Vol. 224, 1994, pp. 253–259.

[21]Armenise, I., Capitelli, M., Celiberto, R., Colonna, G., Gorse, C., and Lagana, A. "The Effect of $N + N_2$ Collisions on the Non-Equilibrium Vibrational Distributions of Nitrogen under Reentry Conditions," *Chemical Physics Letters*, Vol. 227, 1994, pp. 157–163.

[22]Hindmarsh, A. C., "ODE Solvers for Use with the Method of Lines," Lawrence Livermore Lab., UCRL-85293, Preprint, Livermore, CA, March 1981.

[23]Boyd, I. D., Candler, G. V., and Levin, D. A., "Dissociation Modeling in Low Density Hypersonic Flows of Air," *Physics of Fluids*, Vol. 7, No. 7, 1995, pp. 1757–1763.